International Symposium
On Turbulence and Shear Flow
Phenomena (TSFP-8)
August 28 - 30, 2013 Poitiers, France



# SCALE INTERACTIONS IN THE FAR-FIELD OF A TURBULENT MIXING LAYER

**Oliver R.H. Buxton**
Department of Aeronautics
Imperial College London, UK
o.buxton@imperial.ac.uk

**Bharathram Ganapathisubrmani**
Aerodynamics and Flight Mechanics Research Group
The University of Southampton, UK
g.bharath@soton.ac.uk

## ABSTRACT

The interaction between the large and small scales in the self-similar region of a nominally two-dimensional planar mixing layer is examined at two different Reynolds numbers, $Re_\lambda \approx 260$ and $Re_\lambda \approx 470$ (where $Re_\lambda$ is the Reynolds number based on Taylor microscale). Particle image velocimetry experiments were performed at two different resolutions, one that captures the range from integral scale ($L$) to Taylor microscale ($\lambda$) and the other that captures the range from Taylor microscale to the Kolmogorov length scale ($\eta$), simultaneously. It is found that the amplitude of the small-scale fluctuations (scales $< \lambda$) is modulated by the large-scale velocity fluctuations (scale $> \lambda$). Negative large-scale fluctuations (i.e. large-scale fluctuations that are less than the local mean) are found to coincide with regions where an increase in the amplitude of the small-scale fluctuations is found. This magnitude amplifying effect, of the small scales by the large scales, is found to increase with the magnitude of the large-scale fluctuations. It is also observed that there is a phase lag in the amplification of the small scale fluctuations by the larger scales. This phase lag can be interpreted to be the effect of large-scale spanwise roller-type structures that leave a wake of the finest scales behind them. The amplitude modulation, which is representative of the interaction between the large and the small scales, is shown to be Reynolds number dependent with the interaction marginally increasing in the Reynolds number range examined.

## INTRODUCTION

Turbulence is known to be a multi-scale problem, in which energy is transferred from the mean flow into turbulent kinetic energy at large scales and dissipated into heat at the small scales via a mean cascade of energy from the large to the small scales (Richardson, 1926; Batchelor & Townsend, 1949; Kolmogorov, 1962). It has long been suggested that the small scales of turbulent flows are universal, but there is a distinct interaction between the large and small scales. Some recent results, primarily in wall-bounded turbulent shear flows, point to the significance of these interactions (Priyadarshana *et al.*, 2007; Kholmyansky & Tsinober, 2008; Mathis *et al.*, 2009*a*,*b*). However, very little information is available on these interactions in other forms of shear flows. In this study, we aim to examine the nature of this interaction between large- and small-scale velocity fluctuations in a turbulent free shear flow. Winant & Browand (1974) stated that "the region between two parallel streams moving at different speeds is the simplest free shear flow which can be considered" and thus a planar mixing layer is investigated in this study.

A variety of researchers have examined the small scales in different types of turbulent flows (for example, Siggia 1981; Jiménez *et al.* 1993; Vincent & Meneguzzi 1994; Mullin & Dahm 2006. Results indicate that the small-scale structures are in the form of "worms" (for enstrophy) surrounded by "sheets" of dissipation. These small-scale structures are approximately 6-10$\eta$ (where $\eta$ is the Kolmogorov scale) in diameter (or thickness) and extend up to Taylor microscale ($\lambda$) in length (or size). Therefore, the size of these structures is substantially smaller than the integral scale ($L$) of the flow. Researchers have also noted that these tubes and sheets appear to be concentrated around larger scale structures (that are larger than Taylor microscale). However, the exact nature of this relationship between dissipative scale structures and larger scale flow structures remains unknown.

The study of Bandyopadhyay & Hussain (1984) was the first study (and perhaps the only) that presented an examination of the interaction between large and small scales in several different shear flows, including wall-bounded shear flows such as boundary layers and free shear flows such as mixing layers, wakes and jets. The authors examined short time correlations between the low and high frequency components of hot wire time series data. Correlations were made between the low pass filtered (low frequency) time series data with the envelope of the high frequency component and found a significant degree of coupling between the scales across all shear flows. This coupling between the scales was observed to be maximised when the high frequency and low frequency signals were concurrent. Of the shear flows studies it was found that there is a 180° phase shift in this coupling for mixing layers and boundary layers only. Subsequently, a significant

amount of work has been done examining the interaction between scales in wall-bounded shear flows.

Hutchins & Marusic (2007) observed that the large-scale structures in turbulent boundary layers tended to modulate the amplitude of the small-scale near wall fluctuations. This observation was expanded upon by Mathis, Hutchins & Marusic (2009*a*). The authors split the streamwise velocity fluctuations' signal into large and small-scale components (low and high wavenumber components) with a spectral filter and then applied the Hilbert transform to determine the envelope for the small-scale fluctuations. By correlating the large-scale fluctuations with the low pass filtered envelope of the small-scale fluctuations they discovered that near the wall large-scale high speed regions, i.e. positive large-scale fluctuations, carry intense superimposed small-scale fluctuations. They thus determined that regions of positive large-scale fluctuations are responsible for amplifying the magnitude of the small-scale fluctuations near the wall. Mathis *et al.* (2009*b*) found that a similar amplitude modulation effect of the small-scale fluctuations by the large-scale fluctuations could be observed in a series of other wall bounded shear flows, such as pipe and channel flows. Recently, this amplitude modulation effect has also been captured in conditional analyses performed based on wall shear-stress (Hutchins *et al.* 2011).

In this study, we examine the interactions between large- and small-scale velocity fluctuations in the self-similar region of a turbulent mixing layer. Particle image velocimetry (PIV) experiments were performed at two different resolutions, one that captures the range from integral scale ($L$) to Taylor microscale ($\lambda$) and the other that captures the range from Taylor microscale to the Kolmogorov length scale ($\eta$), simultaneously. This data is then utilised to explore the interactions between the large and small scales.

## EXPERIMENTAL METHODS

The experimental data for this study was acquired by Buxton (2011), in which full details of all the experimental methods and a full uncertainty analysis are presented. Particle image velocimetry (PIV) measurements were performed in the self-similar region of a nominally two-dimensional planar mixing layer in a water channel, 100 plate thicknesses downstream of the splitter plate trailing edge used to separate the high speed ($U^{\infty}_{\mathrm{HS}}$) and low speed ($U^{\infty}_{\mathrm{LS}}$) streams. The splitter plate had a 4° triangular trailing edge appended to it in order to generate the mixing layer. The measurement location was chosen as it was within the self similar region of the mixing layer (Buxton, 2011), meaning that the turbulence is fully developed, and the mixing layer is not constrained by the sidewall boundary layers, which is the case further downstream in the facility. The Reynolds number of the mixing layer based on convection velocity ($U_c = [U^{HS}_{\infty} + U^{LS}_{\infty}]/2$, where $U^{HS}_{\infty}$ and $U^{LS}_{\infty}$ are the freestream velocities on the high- and low-speed sides of the mixing layer, respectively) and the splitter plate thickness is, $Re_h = 5020$, and the Reynolds number based on the Taylor microscale is, $Re_\lambda \approx 260$ at the measurement location.

One camera was placed above the water channel and fitted with a 50 mm lens, providing a large-scale field of view (FOV) by imaging through a semi-submerged perspex sheet, and three cameras fitted with 105 mm lenses were placed beneath the water channel, providing small-scale FOVs that are spatially embedded within the large-scale FOV, and captured simultaneously. In order to maintain the synchronisation between all four cameras and the laser, data was acquired at a rate of 0.3 Hz, and immediately written to disk. A suitable separation between the two laser pulses responsible for illuminating the PIV plane, $\Delta t$, for both the top camera (low resolution vector field) and the bottom cameras (high resolution vector fields) was found to be 800 $\mu$s, giving mean streamwise pixel displacement of approximately 25 pixels for the bottom cameras and about 4 pixels for the top camera.

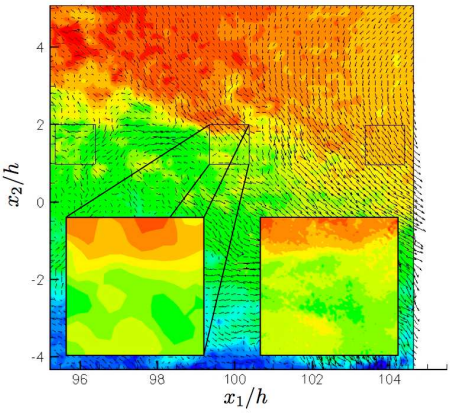


Figure 1. Example PIV vector fields. The contours are of $U_1$, the streamwise velocity, and the vectors have components of $(U_1 - U_c)$ and $U_2$ (with only alternate vectors displayed for ease of presentation), the cross-stream velocity. The insets show a close up of the $U_1$ contours of the centre high resolution field of view from the low resolution vector field (left) and high resolution vector field (right).

The spatial resolution of the large-scale FOV is approximately $12\eta$, where $\eta = (\nu^3/\langle\varepsilon\rangle)^{1/4}$ is the Kolmogorov length scale, whereas that for the small-scale FOV is approximately $1.4\eta$ (with a vector spacing of $0.7\eta$ due to the 50% interrogation window overlap in the PIV processing algorithm). The mean rate of dissipation within the flow, $\langle\varepsilon\rangle$, was computed from the two-dimensional velocity gradient tensor of the small-scale FOVs using the assumption of local axisymmetry (George & Hussein, 1991). Figure 1 shows the location of the three high resolution FOVs within the low resolution FOV. The contours are of $U_1$ and the vectors have components of $(U_1 - U_c)$ and $U_2$ from the low resolution FOV. The left inset shows contours of $U_1$ from the low resolution FOV in the region encompassed by the central high resolution FOV and the right inset shows the contours of $U_1$ from the high resolution FOV itself. It can be seen that there is an excellent agreement between the two.

## DISCUSSION AND RESULTS

The Taylor length scale can be considered to "anchor" the dissipation spectrum, as this is typically the length scale at which the dissipation spectrum is observed to peak, hence $\lambda$ is a suitable cut-off length scale with which to examine the interaction between the large-scale and small-scale fluctuations. The large-scale low-resolution FOV is thus filtered to remove all contributions to the fluctuations at

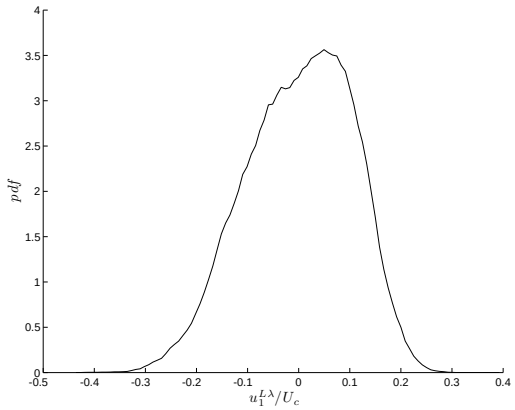


(a)

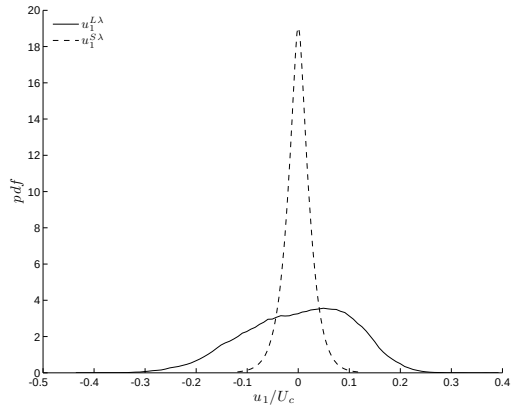


(b)

Figure 2. (a) $pdf$s of $u_1^{L\lambda}$ fluctuations. (b) The dashed line is a $pdf$ of the $u_1^{S\lambda}$ fluctuations and the solid line is the $pdf$ of $u_1^{L\lambda}$ from figure 2(a).

length scales smaller than $\lambda$ (Note that this $\lambda$ is calculated from the small-scale high-resolution FOV). Conversely the small-scale high-resolution FOVs are filtered to remove the contribution of all fluctuations at length scales greater than $\lambda$.

The separation of the scales is achieved by means of a running mean filter. For the large-scale low-resolution FOV the filter is used in low pass form with all the scales smaller than the Taylor microscale filtered out. For the small-scale high-resolution FOV the data is high-pass filtered with all scales greater than the Taylor micro-scale filtered out. The low frequency part and the "$\Lambda < \lambda$" part sum to give the original signal, i.e. $u_1^{S0}(x_1) + u_1^{S\lambda}(x_1) = u_1^{S}(x_1)$. The same filter was also applied to the $u_2$ fluctuations in both the small-scale and large-scale FOVs.

Figure 2(a) shows probability density functions ($pdf$s) of the large-scale streamwise velocity fluctuations produced from the large-scale FOV in regions encompassing the small-scale FOVs ($u_1^{L\lambda}$). Although the fluctuations, by definition, have zero means the $pdf$ is negatively skewed meaning that the modal fluctuations at large scales are positive, but that the negative fluctuations have a greater variance, i.e. there exist higher magnitude negative fluctuations than positive ones. The position of the small-scale FOVs is slightly towards the high speed side of the location of peak mean Reynolds stresses. A $pdf$ generated from all the data in

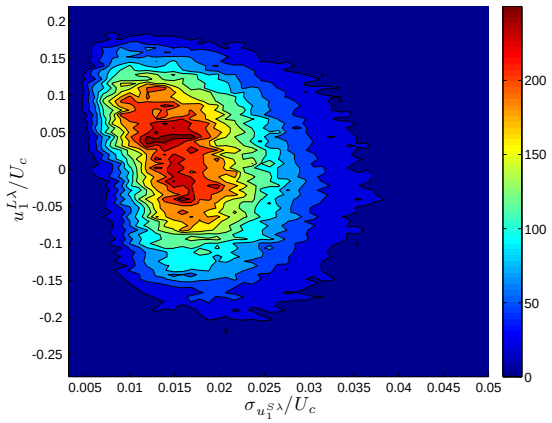


Figure 3. Joint $pdf$ between variance of $u_1^{S\lambda}$ and the representative larger scale fluctuation, $u_1^{L\lambda}$. The colour bar indicates the contour levels for the joint $pdf$.

the high-speed side of the large-scale FOV (this is chosen based on the location of the peak in the Reynolds shear stress profile) shows this same negative skewness, whereas a $pdf$ generated from all the data in the low-speed side of the large-scale FOV shows a positive skewness. Finally, a $pdf$ constructed from all the data in the large-scale FOV shows that the $u_1$ fluctuations have a modal value of zero, and although not Gaussian, has zero skewness. This suggests that a small proportion of high magnitude fluctuations, rather than the smaller modal fluctuations, are at least partially responsible for retarding the flow on the high speed side of the mixing layer and accelerating it on the low speed side. These three $pdf$s are not shown for brevity.

Figure 2(b) shows the $pdf$ of the small-scale fluctuations ($u_1^{S\lambda}$) as the dashed line and the $u_1^{L\lambda}$ $pdf$ of figure 2(a) as the solid line, for reference. In contrast to the large scales, the small-scale fluctuations have a skewness of zero and closely resemble the large-scale fluctuations from across the entire span of the mixing layer. The range of these fluctuations is also significantly less, reflecting their lower energy content. Figures 2(a)&(b) suggest that the retardation of the flow on the high speed side and acceleration on the low speed side is further a large-scale phenomenon that exists only at length scales greater than the Taylor microscale.

The relationship between the large- and small-scale fluctuations can now be be explored using the filtered forms of the large- and small-scale fluctuations. Statistics of the small scales conditioned on the strength/sign of the large scales and vice-versa can be computed. We first examine the interaction by computing the joint probability density function ($pdf$) between $u_1^{L\lambda}$ and the magnitude of the small-scale fluctuations. For a box of size $\lambda \times \lambda$, the large-scale fluctuation value at the centre of this box is chosen to represent the strength of the large-scale fluctuations. The magnitude of the small-scales is computed as the variance of the small-scales within this box ($\sigma_{u_1^{S\lambda}}$).

Figure 3 shows the above-mentioned joint $pdf$. It can be seen in this figure that particularly within regions of highest probability, there is a clear slope towards higher small-scale variance and negative $u_1^{L\lambda}$. There is a tendency for larger-scale negative fluctuations to increase the amplitude of the finer-scale fluctuations. This suggests that both the magnitude and the sign of the large-scale fluctuation,

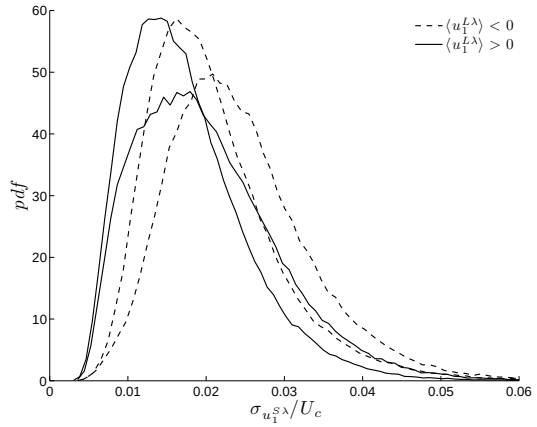


Figure 4. $pdf$s of variance of $u_1^{S\lambda}$ conditioned on the sign of $u_1^{L\lambda}$ computed over a streamwise trace. The $pdf$s with higher peaks are produced from a mixing layer with $Re_\lambda \approx 260$ and the $pdf$s with lower peaks are produced from a mixing layer with $Re_\lambda \approx 470$.

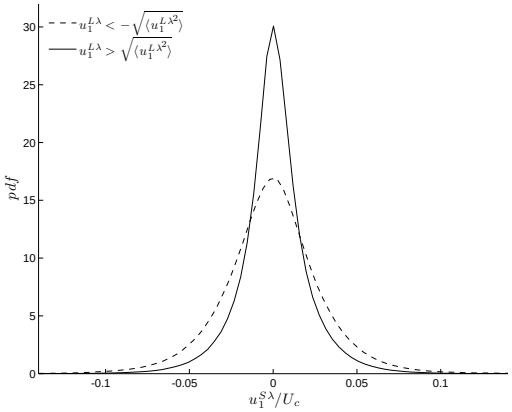


Figure 5. $pdf$ of $u_1^{S\lambda}$ fluctuations conditioned on high magnitude $u_1^{L\lambda}$ fluctuations at $Re_\lambda \approx 260$.

$u_1^{L\lambda}$, are important in determining the intensity of the finer scale fluctuations. This feature has also been observed in the amplitude modulation effects of wall-bounded flows. However, this observed feature is confined to the outer region of the boundary layer. The study of Mathis *et al.* (2009*a*) showed that there is an increase in the amplitude of the small-scale fluctuations in regions for which the large-scale fluctuation is positive in the near-wall region of boundary layers. Mathis *et al.* (2009*b*) presented similar findings in channel and pipe flows. In this study, presenting data from a free shear layer, it can be seen that the opposite is true and that the amplitude of the small-scale fluctuations is increased in regions in which the large-scale fluctuation is negative (i.e. a large low-momentum structure) and reduced in regions in which the large-scale fluctuation is positive (i.e. a large high-momentum structure). This feature is further explored by computing the conditional $pdf$ of the variance of $u_1^{S\lambda}$.

Figure 4 shows $pdf$s of the variance of $u_1^{S\lambda}$ conditioned on $u_1^{L\lambda}$, i.e. shows the relative magnitude of the small-scale fluctuations conditioned upon the large scale fluctuations. The dashed lines are $pdf$s conditioned on $u_1^{L\lambda} < 0$, i.e. negative instantaneous larger scale fluctuations and the solid lines are conditioned on $u_1^{L\lambda} > 0$. Data from two different Reynolds numbers are shown; the $pdf$s with the higher modal peaks are from the mixing layer for which $Re_\lambda \approx 260$ and the $pdf$s with the lower modal peaks are the mixing layer at $Re_\lambda \approx 470$, and a correspondingly higher $U_c$. For both Reynolds numbers, the peak location of the $pdf$ is at a higher value for negative larger scale fluctuations than for positive fluctuations. This suggests that the larger scale negative fluctuations have an amplitude amplifying effect on the finer scales. The higher Reynolds number $pdf$s have broader tails, that stretch to a much greater extent, and correspondingly lower modal peaks. The variance of the $u_1^{S\lambda}$ signal is also analogous to the turbulent kinetic energy contained within these finer scales, hence it is unsurprising that the higher Reynolds number data contains a higher proportion of high variance signals.

The modal value for the $pdf$s conditioned on $u_1^{L\lambda} > 0$ in figure 4 is similar for both Reynolds numbers, although there is a broader peak for the higher Reynolds number case. This is not the case for the $pdf$s conditioned on $u_1^{L\lambda} < 0$. There is a distinct shift towards higher variance for the higher Reynolds number case. There is thus also a Reynolds number effect in the interaction between the larger and finer scale fluctuations, with higher Reynolds number encouraging a greater increase in the amplitude of the small scales by large-scale negative streamwise velocity fluctuations.

Thus far, we have established the variance in small scale fluctuations is amplified by the large scale fluctuations. However, the distribution of the small scale fluctuation that contributes to the variance is not known. In order to explore this feature, we present the conditional $pdf$ of the small scale fluctuation conditioned on the value of the large scale fluctuation. We are specifically interested in regions in which the large scale fluctuations are strong. Figure 5 shows the $pdf$ of $u_1^{S\lambda}$ conditioned on $u_1^{L\lambda}$. The dashed line $pdf$s are produced from high magnitude negative fluctuations and the solid line $pdf$s are produced from high magnitude positive fluctuations. It can be seen that conditional $pdf$s for strong positive fluctuations exhibit a different behaviour to that of the conditional $pdf$s for strong negative fluctuations. The tails of the $u_1^{S\lambda}$ $pdf$s conditioned on negative $u_1^{L\lambda}$ in figure 5 are significantly broader than those conditioned on positive fluctuations. This leads to a correspondingly lower modal peak, although the mode remains (along with the mean) at zero. It can thus be concluded that high magnitude, large-scale negative fluctuations have an effect of increasing the activity in fluctuations smaller than the Taylor microscale.

Another way to examine the influence of the large scales on the small scale fluctuations (and vice-versa) is to calculate the dissipation in the small scale field of view and condition the large scale fluctuation on the value of the dissipation. Figure 6 shows $pdf$s of the large-scale fluctuations of $u_1^{L\lambda}$ conditioned on the mean dissipation rate, $\langle \varepsilon^{S\lambda} \rangle$, from the small-scale FOV. The solid line $pdf$ is produced from regions encompassing small-scale FOVs that instantaneously have a mean rate of dissipation that is higher than the global mean. It can be seen that these large-scale fluctuations have a modal value of close to zero and negative skewness that is significantly smaller than that for the overall $pdf$ of figure 2. On the other hand the dashed line $pdf$, constructed from regions encompassing the small-scale FOVs with a mean rate of dissipation that is lower than

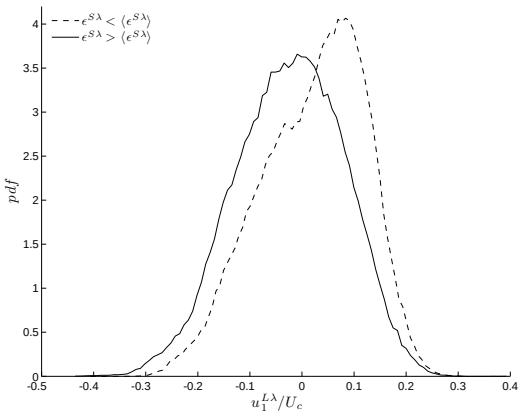


Figure 6. $pdf$s of $u_1^{L\lambda}$ fluctuations conditioned on the rate of dissipation of turbulent kinetic energy, $\varepsilon$, in the small-scale FOVs.

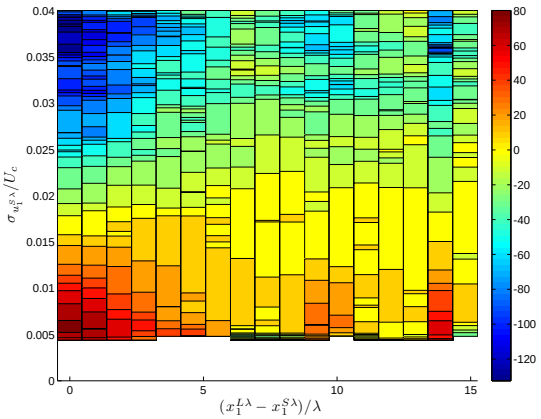


Figure 7. (a) Contour plot showing the percentage difference between the $pdf$ conditioned on $u_1^{L\lambda} > 0$ and the $pdf$ conditioned on $u_1^{L\lambda} < 0$ produced using the $u_1^{L\lambda}$ data in the streamwise domain of each band downstream of the $u_1^{S\lambda}$ data in the upstream high resolution FOV.

the global mean, shows a positive modal value and a significant degree of negative skewness.

This means that regions of high dissipation are more likely to be found in high magnitude negative large-scale velocity fluctuations and regions of low dissipation are more likely to be found in large magnitude positive large-scale fluctuations. Roshko (1976) states that in the development region of the mixing layer the large scales are unaffected by the small scales and the dissipation. Figure 6 shows that this is not the case in the self similar region of a mixing layer, with the dissipation (a small-scale quantity) clearly correlated with the distribution of the large-scale fluctuations. The cause-and-effect relationship of the impact of large- on small-scale and vice-versa is not clear as this requires us to examine the spatio-temporal evolution of these conditional statistics. However, there is evidence that the small scales have a significant impact on the large scales and a confirmation of the finding of figure 5 that high activity amongst the small scales is more likely to be found in regions of large-scale negative velocity fluctuations.

Figure 1 shows the locations of the three small-scale FOVs in relation to the large-scale FOV. It can be seen that there is a considerable area in the large-scale FOV downstream of two small-scale FOVs (upstream and centre small-scale FOVs). This area in the large-scale FOV, which does not encompass the small-scale FOVs, can be used to examine the history effects or the phase lag between the fine scales within the small-scale FOV and the larger scales in the large-scale FOV. Therefore, we calculate conditional $pdf$s of $\sigma_{u_1^{S\lambda}}$ conditioned on the presence of positive or negative large scale streamwise velocity fluctuations downstream of the fine scale fluctuations. Computation of these $pdf$s is straightforward and follows the same procedure outlined above. However, the condition points (or areas) are now located downstream of the small-scale FOV. Thus these conditional $pdf$s show the behaviour of the finer scale fluctuations that persist in the "wake" of the large scales. The region downstream of the most upstream small-scale FOV is split into streamwise sections of length $2\lambda$ (which is the streamwise extent of the small-scale FOV) and $pdf$s of $\sigma_{u_1^{S\lambda}}$ are computed conditioned on the sign of $u_1^{L\lambda}$ downstream of the small-scale FOV.

Figure 7 shows contours of the percentage difference (based on the $pdf$ conditioned on positive fluctuations (*c.f.* the solid lines of figure 4)) between $pdf$s calculated for $u_1^{L\lambda} > 0$ and $u_1^{L\lambda} < 0$ as a function of both the relative downstream locations and $\sigma_{u_1^{S\lambda}}$, given by:

$$pdf\ \%\ \text{difference} = 100 \times \frac{pdf|_{u_1^{L\lambda}>0} - pdf|_{u_1^{L\lambda}<0}}{pdf|_{u_1^{L\lambda}>0}} \quad (1)$$

Each band in the figure is offset by a distance of $\lambda$, up to a maximum downstream distance of $\approx 16\lambda$, which corresponds to the streamwise extent of the large-scale FOV. A positive value of the difference indicates that the bin that corresponds to a given relative streamwise position and $\sigma_{u_1^{S\lambda}}$ is dominated by events for which $u_1^{L\lambda} > 0$ at that relative streamwise position. Conversely, a negative value indicates that $\sigma_{u_1^{S\lambda}}$ is dominated by events for which $u_1^{L\lambda} < 0$ at that relative streamwise position. The data extracted along $x_1^{L\lambda} - x_1^{S\lambda} = 0$ in the figure corresponds to the difference between the $pdf$ conditioned on $u_1^{L\lambda} > 0$ and the $pdf$ conditioned on $u_1^{L\lambda} < 0$ of figure 4.

At the measurement location, in the high Reynolds number case, the Kolmogorov time scale is approximately 33 ms compared to a time of approximately 38 ms required to convect a distance of $2\lambda$ at the mean velocity at the measurement location. This suggests that the small scales respond quickly to the passage of a region of sustained negative streamwise velocity fluctuations in the large scales. It can be postulated that the mechanism by which the amplitude of the finest scales is increased by a region of negative $u_1^{L\lambda}$ downstream is to do with a local increase in the Reynolds number as the velocity is increased. However, it is not clear whether the amplitude modulation is causal due to the Eulerian nature of our data, but a local increase in Reynolds number would also account for the reduction in influence of the smallest scales.

Figure 7 shows that the effect of the larger scales on the finest scales can be seen to be at its greatest when the large scale negative fluctuations are concurrent with the finest scales, illustrated by the large negative value contours for

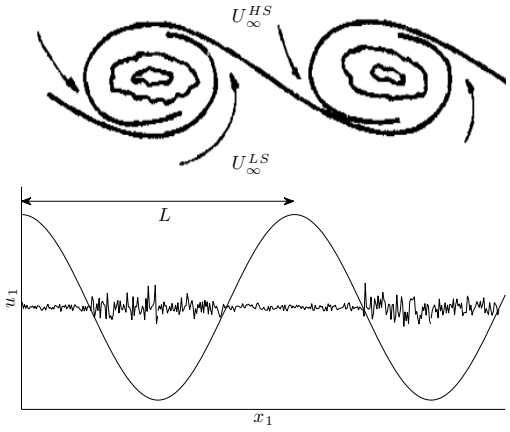


Figure 8. Illustrative representation highlighting the zones of interaction between larger and finer scales in the mixing layer. The integral length scale is marked in the figure and in the current study the ratio between the integral scale and the Taylor microscale, $L/\lambda = 21$ (for $Re_\lambda \approx 260$).

higher values of $\sigma_{u_1^{S\lambda}}$ at the streamwise origin. This effect steadily decreases with increasing downstream distance of the conditional point up to $x_1^{L\lambda} - x_1^+ \approx 8\lambda$ where it increases again reaching a secondary peak/valley at the farthest downstream location at $x_1^{L\lambda} - x_1^+ = 15\lambda$.

As mentioned previously, figure 7 shows an increase in this amplitude modulation at a distance of $\approx 15\lambda$ downstream of the small-scale FOV, although it can still be seen that negative large-scale fluctuations are responsible for increasing the finest scale activity as there is no sign change present. At this location downstream, the amplitude of the finest scales is correlated to a negative velocity fluctuation.

The above-mentioned observations on amplitude modulation and the phase lag can be reconciled through a physical mechanism that involve the passage of integral scale sized structures that leave a "wake" of fine scales behind them. Figure 8 shows a schematic representation of this physical mechanism. The top of the figure shows two adjacent typical spanwise rollers that are the larger scales in the mixing layers (Winant & Browand 1974; Brown & Roshko 1974). These structures are of the size of integral scale ($L$) which is approximately equal to $20\lambda$ in the current study. The bottom plot in figure 8 shows a trace of the streamwise velocity fluctuation of the larger scales taken along the line shown in the top plot; similar to those presented in Loucks & Wallace (2012). This line plot shows that larger scale streamwise velocity fluctuations are positive upstream of a roller and steadily decreases through the roller reaching a minimum at the centre of a roller and increases beyond this point until the beginning of the adjacent roller. This velocity signature is derived from the entrainment of high-speed fluid (from the high-speed side) upstream of the roller and entrainment of low-speed fluid (from the low-speed side) downstream of the roller. The bottom of the figure also shows the fluctuations of the finest scales through the same line shown in the top plot. This signature shows that the finest scales are amplified within the roller and are attenuated in the shear layers that connect the adjacent rollers.

## REFERENCES

Bandyopadhyay, P.R. & Hussain, A.K.M.F. 1984 The coupling between scales in shear flows. *Phys. Fluids* **27** (9), 2221–2228.

Batchelor, G.K. & Townsend, A.A. 1949 The nature of turbulent motions at large wave-numbers. *Proc. R. Soc. Lond. A* **199**, 238–255.

Brown, G.L. & Roshko, A. 1974 On density effects and large structure in turbulent mixing layers. *J. Fluid Mech.* **64**, 775–816.

Buxton, O.R.H. 2011 Fine scale features of turbulent shear flows. PhD thesis.

George, W.K. & Hussein, H.J. 1991 Locally axisymmetric turbulence. *J. Fluid Mech.* **233**, 1–23.

Hutchins, N. & Marusic, I. 2007 Large-scale influences in near-wall turbulence. *Phil. Trans. R. Soc. Lond.* **365**, 647–664.

Hutchins, N., Monty, J.P., Ganapathisubramani, B., Ng, H. & Marusic, I. 2011 Three-dimensional conditional structure of a high Reynolds number turbulent boundary layer. *J. Fluid Mech.* **673**, 255–285.

Jiménez, J., Wray, A.A., Saffman, P.G. & Rogallo, R.S. 1993 The structure of intense vorticity in isotropic turbulence. *J. Fluid Mech.* **255**, 65–90.

Kholmyansky, M. & Tsinober, A. 2008 Kolmogorov 4/5 law, nonlocality, and sweeping decorrelation hypothesis. *Phys. Fluids* **20** (041704), 1–4.

Kolmogorov, A.N. 1962 A refinement of previous hypotheses concerning the local structure of turbulence in a viscous incompressible fluid at high Reynolds number. *J. Fluid Mech.* **13**, 82–85.

Loucks, R.B. & Wallace, J.M. 2012 Velocity and velocity gradient based properties of a turbulent plane mixing layer. *J. Fluid Mech.* **doi:10.1017/jfm.2012.103**, 1–40.

Mathis, R., Hutchins, N. & Marusic, I. 2009*a* Large-scale amplitude modulation of the small-scale structures in turbulent boundary layers. *J. Fluid Mech.* **628**, 311–337.

Mathis, R., Monty, J.P., Hutchins, N. & Marusic, I. 2009*b* Comparison of large-scale amplitude modulation in turbulent boundary layers, pipes and channel flows. *Phys. Fluids* **21** (111703), 1–4.

Mullin, J.A. & Dahm, W.J.A. 2006 Dual-plane stereo particle image velocimetry measurements of velocity gradient tensor fields in turbulent shear flow II. Experimental results. *Phys. Fluids* **18** (035102), 1–28.

Priyadarshana, P.J.A., Klewicki, J.C., Treat, S. & Foss, J.F. 2007 Statistical structure of turbulent-boundary-layer velocity - vorticity products at high and low Reynolds numbers. *J. Fluid Mech.* **570**, 307–346.

Richardson, L.F. 1926 Atmospheric diffusion shown on a distance-neighbour graph. *Proc. R. Soc. Lond. A* **110** (756), 709–737.

Roshko, A. 1976 Structure of turbulent shear flows: a new look. *AIAA J.* **14** (10), 1349–1357.

Siggia, E.D. 1981 Numerical study of small-scale intermittency in three-dimensional turbulence. *J. Fluid Mech.* **107**, 375–406.

Vincent, A. & Meneguzzi, M. 1994 The dynamics of vorticity tubes in homogeneous turbulence. *J. Fluid Mech.* **258**, 245–254.

Winant, C.D. & Browand, F.K. 1974 Vortex pairing: the mechanism of turbulent mixing-layer growth at moderate Reynolds number. *J. Fluid Mech.* **63**, 237–255.